# Phase Stability of Bi-2(V1-xMEx)O5.5+delta (ME = Li and Ag, x=0.05 and 0.1)

AUTHOR(S):

Taninouchi, Yu-ki; Uda, Tetsuya; Ichitsubo, Tetsu; Awakura, Yasuhiro; Matsubara, Eiichiro

CITATION:

Taninouchi, Yu-ki ...[et al]. Phase Stability of Bi-2(V1-xMEx)O5.5+delta (ME = Li and Ag, x=0.05 and 0.1). MATERIALS TRANSACTIONS 2010, 51(3): 561-566

ISSUE DATE:

2010

URL:

http://hdl.handle.net/2433/148407

*Materials Transactions*, Vol. 51, No. 3 (2010) pp. 561 to 566


**EXPRESS REGULAR ARTICLE**

# Phase Stability of $Bi_2(V_{1-x}ME_x)O_{5.5+\delta}$ (ME = Li and Ag, $x = 0.05$ and 0.1)

Yu-ki Taninouchi*, Tetsuya Uda, Tetsu Ichitsubo, Yasuhiro Awakura and Eiichiro Matsubara

*Department of Materials Science and Engineering, Kyoto University, Kyoto 606-8501, Japan*

The phase transition of high oxide-ion conductor $Bi_2(V_{1-x}ME_x)O_{5.5+\delta}$ (ME = Li and Ag, $x = 0.05$ and 0.1) and its long-term phase stability against thermal decomposition have been studied. The transition behavior was determined by differential scanning calorimetry (DSC) as well as high-temperature X-ray diffraction (HT-XRD) analysis. The observed thermal and structural changes during temperature scans reveal the temperature dependence of electrical conductivity. Li- and Ag-doping do not sufficiently suppress thermal decomposition at intermediate temperatures between 400 and 600°C. In particular, partial decomposition was detected in $Bi_2(V_{0.9}Ag_{0.1})O_{5.3}$ during a temperature scan by HT-XRD analysis, which explains the distinct change in electrical conductivity. We have generated pseudo-binary phase diagrams for $Bi_2(V_{1-x}ME_x)O_{5.5+\delta}$ based on the X-ray diffraction analysis of powders annealed for 200 h and differential thermal analysis. The thermodynamically stable region of $Bi_2(V_{1-x}ME_x)O_{5.5+\delta}$ is not sufficiently expanded by Li- and Ag-doping. At around 500°C, $Bi_2(V_{1-x}ME_x)O_{5.5+\delta}$ is metastable, although it shows the highest oxide-ion conductivity among solid oxides. [doi:10.2320/matertrans.M2009348]

(Received October 13, 2009; Accepted December 8, 2009; Published February 25, 2010)

***Keywords:*** *BIMEVOX, $Bi_2VO_{5.5}$, phase transition, phase stability, phase decomposition, lithium, silver*

## 1. Introduction

$Bi_2(V_{1-x}ME_x)O_{5.5+\delta}$ (ME: dopant metal, $x$: dopant concentration, $\delta$: deviation of oxygen content from original stoichiometry), i.e., BIMEVOX, is a strong candidate for oxide-ion conduction at intermediate temperatures between 400 and 600°C.[1–4] Non-doped $Bi_2VO_{5.5}$ has a single-layer Aurivillius structure and shows three main polymorphs: $\alpha$ (below 450°C), $\beta$ (from 450 to 570°C), and $\gamma$ (above 570°C).[5] Their lattice structures are characterized by an orthorhombic subcell of $a_m = 0.553$, $b_m = 0.561$, and $c_m = 1.528$ nm, i.e., $a \approx 3a_m$, $b \approx b_m$, $c \approx c_m$, $\gamma \approx 90.26°$ for monoclinic $\alpha$, $a \approx 2a_m$, $b \approx b_m$, $c \approx c_m$ for orthorhombic $\beta$, and $a \approx a_m/\sqrt{2}$, $c \approx c_m$ for tetragonal $\gamma$.[6,7] Characteristic superlattice diffraction peaks are observed in the diffraction patterns of $\alpha$- and $\beta$-$Bi_2VO_{5.5}$. $\beta$- and $\gamma$-$Bi_2VO_{5.5}$ exhibit oxide-ion conduction. In particular, the conductivity of $\gamma$-phase is as high as $3 \times 10^{-1}$ S cm$^{-1}$.

The polymorphs of $Bi_2VO_{5.5}$ and their electrical properties are significantly affected by doping. We have reported that the $\gamma$-phases of monovalent-metal-doped $Bi_2VO_{5.5}$ [$Bi_2(V_{1-x}ME_x)O_{5.5+\delta}$; ME = Li and Ag, $x = 0.05$ and 0.1] are stabilized below 570°C and show quite high oxide-ion conductivities at around 500°C.[8] Their oxide-ion conductivities are 0.5–1 $\times 10^{-1}$ S cm$^{-1}$ at 500°C, which are the highest values among solid oxides, and almost the same order of those of $(ZrO_2)_{0.92}(Y_2O_3)_{0.08}$ at around 850°C,[9] of $(CeO_2)_{0.85}(SmO_{1.5})_{0.15}$ at around 750°C,[10] and of $La_{0.8}Sr_{0.2}Ga_{0.8}Mg_{0.115}Co_{0.085}O_3$ at around 600°C.[11]

In the present study, the phase transitions of Li- and Ag-doped $Bi_2VO_{5.5}$ were investigated by differential scanning calorimetry (DSC) and high-temperature X-ray diffraction (HT-XRD) analysis in order to understand the change in the electrical conductivity. Recently, Watanabe[12] reported that $Bi_2VO_{5.5}$ is metastable below 550°C and it decomposes to $BiVO_4$ and $Bi_{3.5}V_{1.2}O_{8.25}$ for 300 h or more. Steil *et al.*[13] also confirmed that $Bi_2VO_{5.5}$ completely decomposes into $BiVO_4$ and $Bi_{3.5}V_{1.2}O_{8.25}$ at 500°C for 7 weeks. The long-term phase stability is the key for the practical use. Therefore, we assessed the phase stabilities of Li- and Ag-doped $Bi_2VO_{5.5}$ and established the phase diagrams.

In this paper, the phases are simply classified as $\alpha$-, $\beta$-, or $\gamma$-phase according to the characteristic superlattice diffraction peaks, irrespective of the symmetry of the unit cell. That is, the orthorhombic phases of $Bi_2(V_{0.95}Li_{0.05})O_{5.4}$ and $Bi_2(V_{0.95}Ag_{0.05})O_{5.4}$ that show characteristic superlattice diffraction peaks of $\alpha$-$Bi_2VO_{5.5}$ are classified as $\alpha$-phases. The tetragonal phases that show characteristic superlattice diffraction peaks of $\beta$-$Bi_2VO_{5.5}$ are classified as $\beta$-phases.

## 2. Experimental

The polycrystalline powders listed in Table 1 were synthesized by the solid-state reaction in air using platinum containers.[8] Appropriate amounts of $Bi_2O_3$ (99.99%; Furuuchi Chemical), $V_2O_5$ (99.9%; Furuuchi Chemical), $Li_2CO_3$ (99.9%; Furuuchi Chemical), and $Ag_2O$ (99%+; Wako) were mixed and then heated at 600°C for 12 h. The ground powders were pelletized at 19.6 MPa, heated again at 800°C (Li5, Ag5, and Ag10) or 700°C (Li10) for 12 h, and then grinded. Before analysis, synthesized powders were kept at 700°C (Li5, Li10, and Ag5) or 750°C (Ag10) for several hours and then quenched in air.

DSC was performed using a Diamond differential scanning calorimeter (PerkinElmer) with platinum containers. Pow-

Table 1 Abbreviations, compositions, and phases of prepared samples. The phases were identified at room temperature from powders quenched from 700°C (Li5, Li10, and Ag10) or 750°C (Ag10).[8]

| Abbreviation | Composition | Phase at room temperature |
|---|---|---|
| Li5 | $Bi_2(V_{0.95}Li_{0.05})O_{5.4}$ | orthorhombic $\alpha$ |
| Li10 | $Bi_2(V_{0.9}Li_{0.1})O_{5.3}$ | tetragonal $\gamma$ |
| Ag5 | $Bi_2(V_{0.95}Ag_{0.05})O_{5.4}$ | orthorhombic $\alpha$ |
| Ag10 | $Bi_2(V_{0.9}Ag_{0.1})O_{5.3}$ | tetragonal $\gamma$ |

*Graduate Student, Kyoto University, Corresponding author, E-mail: taninouchi@t01.mbox.media.kyoto-u.ac.jp

ders were heated and cooled at 10 K min$^{-1}$ between 100 and 700°C in artificial air. HT-XRD analysis was carried out in air using X'Pert PRO MPD (PANalytical, Cu-K$\alpha$ radiation) with an HTK-1200N oven chamber (Anton Paar). The scan rate of the sample temperature was 10 K min$^{-1}$. The sample temperatures were maintained for 5 min at 50°C intervals, and diffraction patterns were collected within 10 min at each temperature.

The long-term phase stability was assessed by carrying out XRD analysis of the powder samples annealed at various temperatures for 200 h in air. Compositions of the annealed powders were determined by measuring the concentration of metallic ions by energy-dispersive X-ray microanalysis (EDX) using JSM-6500F (JEOL), on the assumption that oxygen content follows the stoichiometry evaluated from the valences of the metallic ions. Differential thermal analysis (DTA) was also carried out using DTG-60H (Shimadzu) until the liquid phase appeared. Powders in alumina containers were heated to ~900°C at 10 K min$^{-1}$ in artificial air.

## 3. Results and Discussion

### 3.1 Phase transitions and phase decompositions determined by DSC and HT-XRD analysis

Figure 1 shows the DSC profiles of Li- and Ag-doped $Bi_2VO_{5.5}$ with the reference profile of $Bi_2VO_{5.5}$. As seen in Fig. 1, $Bi_2VO_{5.5}$ shows two endothermic peaks on heating and two exothermic peaks on cooling, corresponding to the transitions between $\alpha$- and $\beta$-phases and $\beta$- and $\gamma$-phases, respectively. Figure 2 shows the HT-XRD profiles on heating, and Fig. 3 shows a summary of the phases confirmed by HT-XRD analysis. We must note that the diffraction intensities shown in Fig. 2 are plotted in the logarithmic scale to clarify the superlattice diffraction peaks and small peaks of secondary phases.

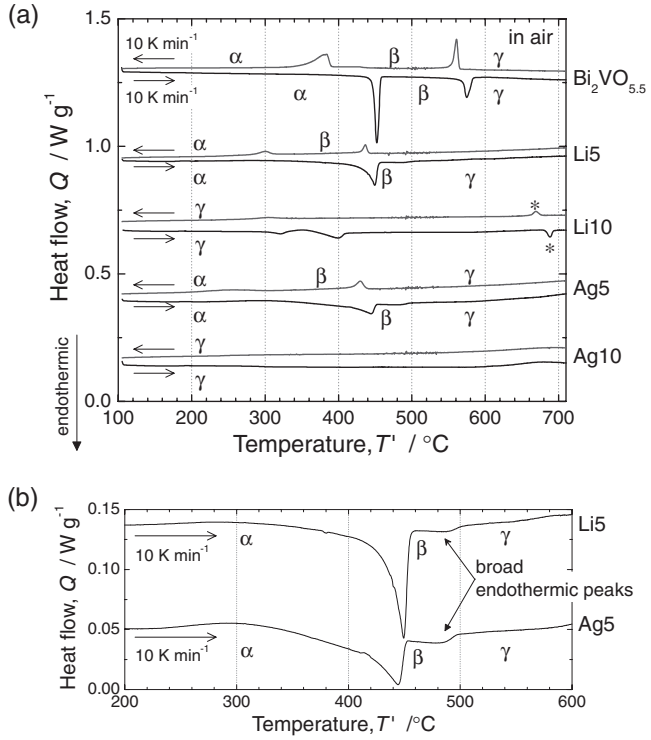


Fig. 1 (a) DSC profiles of Li- and Ag-doped $Bi_2VO_{5.5}$. The profile of $Bi_2VO_{5.5}$ is shown as a reference. Quenched powders were heated and cooled at 10 K min$^{-1}$ in air. In Li10, the peaks denoted by asterisks correspond to the reaction: Li10 ↔ BIMEVOX phase + small amount of liquid. (b) Magnified profiles of Li5 and Ag5 on heating.

The transition between $\alpha$- and $\gamma$-phases passes through the $\beta$-phase in Li5 and Ag5. In the DSC profiles of Li5 and Ag5 on heating, clear endothermic peaks appeared from 400 to 450°C, corresponding to the transition from $\alpha$- to $\beta$-phases ($\alpha/\beta$ transition). It should be noted that the $\beta$-phases of Li5 and Ag5 at 450°C on heating have tetragonal symmetry, as shown in Fig. 2(a) and (c). Very broad and small endothermic peaks were observed for the $\beta/\gamma$ transition at approximately 480°C in DSC profiles. The broad peak can be explained on the basis of the nature of the second-order $\beta/\gamma$ transition in Li5 and Ag5. DSC profiles are consistent with continuous conductivity changes at the $\beta/\gamma$ transition, as shown in Fig. 4.[8] In the DSC profiles of Li5 and Ag5 on cooling, the exothermic peaks at around 420°C correspond to the $\gamma/\beta$ transition. The exothermic peaks corresponding to the $\beta/\alpha$ transition are very small and broad, which indicates that the $\beta/\alpha$ transitions in Li5 and Ag5 proceed gradually.

In Li10 and Ag10, the fundamental diffraction peaks were attributed to the $\gamma$-phase. In the DSC profile of Li10, two endothermic peaks are exhibited in the temperature range from 300 to 420°C. In the same temperature range, the diffraction peaks were broadened as shown in Fig. 3(b) and the conductivity increased in Fig. 4. Considering that the broadened peaks split in the orthorhombic $\alpha$-phase and became a single peak in the tetragonal $\beta$- and $\gamma$-phases, as shown in Fig. 2(a), the broadening of the peaks at 300 and 350°C in Fig. 2(b) is attributed to some structural relaxation induced by the rearrangement of oxygen vacancies and/or dopant Li. A pair of endothermic and exothermic peaks is observed at around 680°C in the DSC profile of Li10, as indicated by asterisks. These peaks correspond to a partial melting of Li10, as explained in the following section. In the case of Ag10, no clear peak is observed in the DSC profiles, although Ag10 shows a slow conductivity jump from 300 to 400°C, as shown in Fig. 4.

Results of the HT-XRD analysis also showed the progress of thermal decompositions in Li10, Ag5, and Ag10 during the temperature scan. In Li10, a very small amount of the secondary phase appeared from 550 to 650°C on heating. Similarly, a small amount of the secondary phase appeared in Ag5. The results are summarized in Fig. 3. In Ag10, a relatively large amount of the secondary phase appeared from 550 to 700°C on heating, as shown in Fig. 2(d). The composition of the secondary phase is estimated to be $Bi_{14}V_5AgO_{34}$. The ratio of the maximum peak of the secondary phase at ~27.1° to that of BIMEVOX at ~28.2°, $I_{SP}/I_{BVO}$, is shown in Fig. 5 as a function of temperature. The amount of secondary phase increases from 550 to 650°C and then decreases from 650 to 700°C. Thus, the distinct change in the conductivity of Ag10 from 540 to 730°C, which is shown in region (i) of Fig. 4, is explained by the decomposition reaction from 540 to 630°C,

$$\text{Ag10} \rightarrow \text{BIMEVOX phase} + \text{secondary phases},$$

and the recomposition reaction from 630 to 730°C,

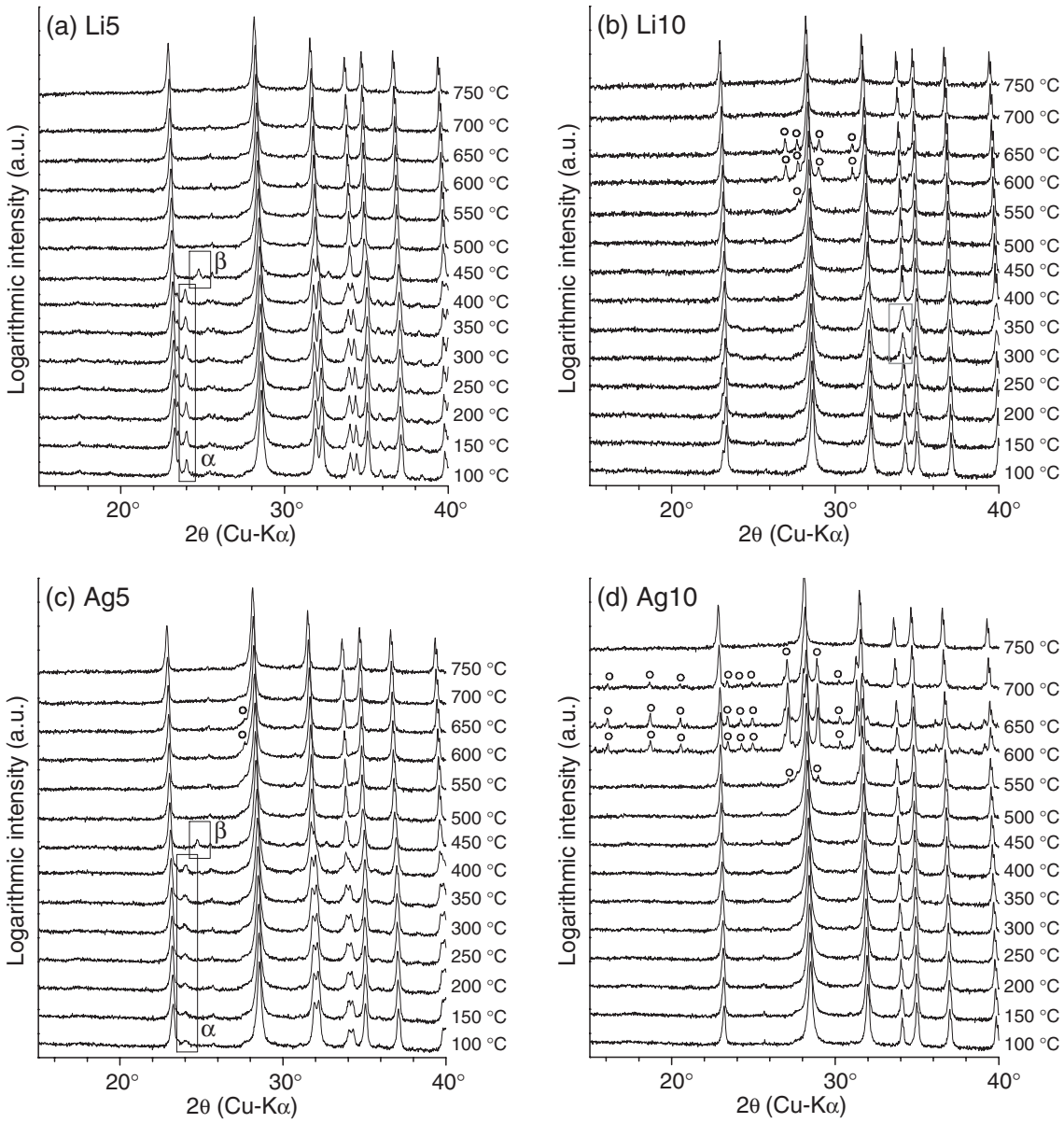


Fig. 2 HT-XRD profiles of (a) Li5, (b) Li10, (c) Ag5, and (d) Ag10 on heating in air. Typical superlattice diffractions of $\alpha$ and $\beta$ are marked in the profiles of (a) Li5 and (c) Ag5. Peak broadening observed at 300 and 350°C in (b) Li10 is indicated by a gray box. The secondary phases that appeared in (b) Li10, (c) Ag5, and (d) Ag10 are indicated by open circles.

$$\text{BIMEVOX phase} + \text{secondary phases} \rightarrow \text{Ag10}.$$

On cooling, a small amount of the secondary phase ($I_{SP}/I_{BVO}$, ~1.5%) appeared below 550°C in Ag10.

The appearance of secondary phases during the HT-XRD analysis indicates the instability of Li- and Ag-doped $Bi_2VO_{5.5}$ at intermediate temperatures. Li and Ag have different ionic radii,[14] Pauling electronegativities,[15] and preferable oxygen coordinations, as summarized in Table 2. However, the transition behavior does not show a large difference between Li- and Ag-doped $Bi_2VO_{5.5}$ at the same dopant concentration. The dopant concentration changes the oxygen content of BIMEVOX to preserve electroneutrality. Thus, the dominant factors that determine the transition behavior of BIMEVOX are dopant and oxygen contents.

### 3.2 Long-term phase stabilities and phase diagrams determined by XRD analysis of annealed powders and DTA

Figure 6 shows the XRD patterns of powders after annealing for 200 h at 500 or 700°C. At 500°C, $Bi_2VO_{5.5}$ is partially decomposed during annealing. The decomposition was also confirmed in doped $Bi_2VO_{5.5}$ at 500°C. In particular, the BIMEVOX phase almost disappeared in annealed Li5. Ag10 annealed at 500°C contained the BIMEVOX phase, $BiVO_4$, and two other phases whose compositions are roughly evaluated as $Bi_{14}V_5AgO_{34}$ and $Bi_3V_2AgO_{10}$ by EDX. In Ag10 annealed at 700°C, a secondary phase exists although the BIMEVOX phase remained as the main phase. EDX indicated that the composition of the secondary phase was $Bi_{14}V_5AgO_{34}$, and the composition of the BIMEVOX phase remained largely

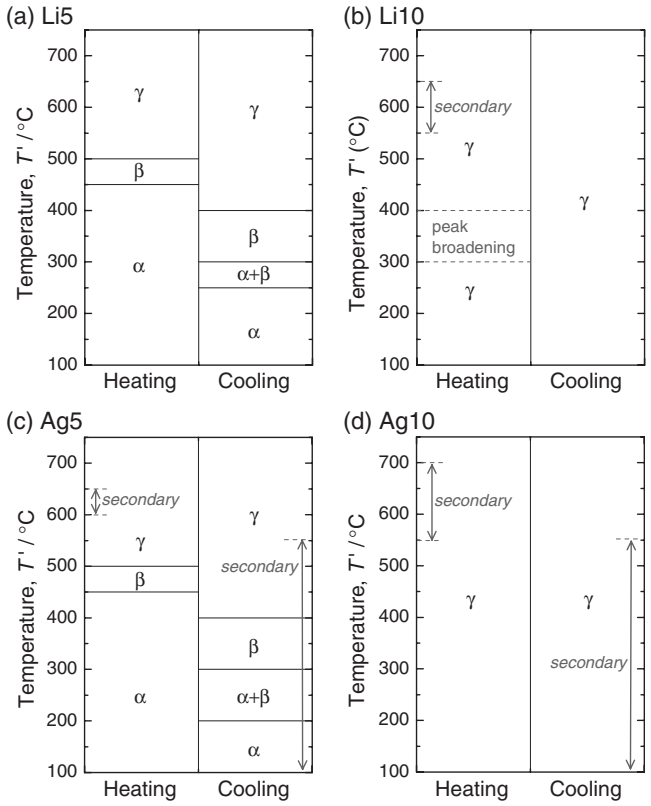


Fig. 3 Summary of the phases in (a) Li5, (b) Li10, (c) Ag5, and (d) Ag10 determined by HT-XRD analysis. The ranges in which secondary phases appeared are indicated by arrows.

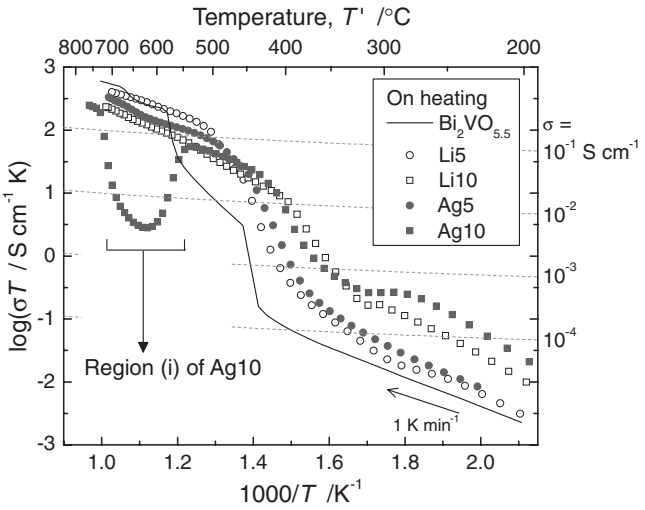


Fig. 4 Reprinted data of changes in electrical conductivity of $Bi_2VO_{5.5}$, Li5, Li10, Ag5, and Ag10.[8] Pellets with Au electrodes were quenched from 800°C ($Bi_2VO_{5.5}$), 700°C (Li5, Li10, and Ag5), or 750°C (Ag10) just before measurements. Samples were heated at 1 K $min^{-1}$ under flowing artificial air. A distinct conductivity change was observed in region (i) for Ag10.

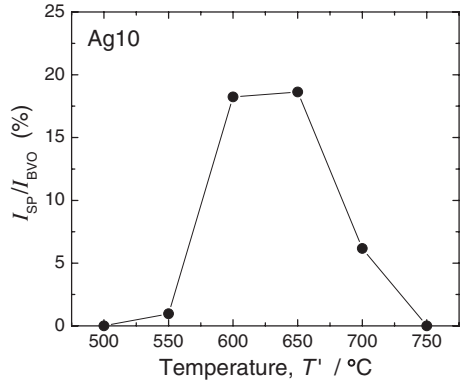


Fig. 5 Variation in the amount of secondary phase in Ag10. $I_{SP}/I_{BVO}$, which is the ratio of the relative intensity of the maximum peak of the secondary phase at ~27.1° shown in Fig. 3(d) to the maximum peak of the BIMEVOX phase, is plotted as a function of temperature.

Table 2 Valences, Shannon ionic radii in 6-fold coordination,[14] Pauling electronegativities,[15] and preferable oxygen coordinations of Li and Ag. Oxygen coordinations in $Li_2O$ (anti-fluorite structure) and $Ag_2O$ (cuprite structure) were regarded as preferable.

| | Valence | Ionic radius (nm) | Electronegativity | Preferable oxygen coordination |
|---|---|---|---|---|
| Li | +1 | 0.076 | 0.98 | tetrahedrally 4-fold |
| Ag | +1 | 0.115 | 1.93 | linearly 2-fold |

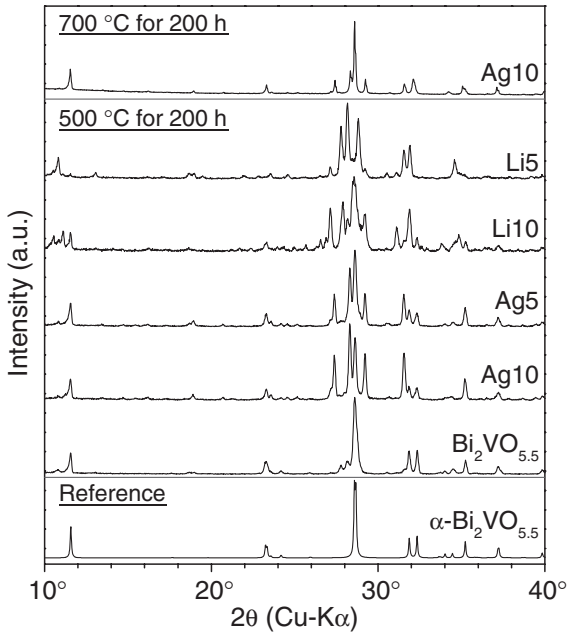


Fig. 6 XRD patterns of powders after annealing at 500 or 700°C for 200 h. The calculated pattern of $\alpha$-$Bi_2VO_{5.5}$ is shown for reference.[7] The composition of the secondary phase in Ag10 annealed at 700°C is determined to be $Bi_{14}V_5AgO_{34}$ by EDX.

unchanged as $Bi_2(V_{0.9}Ag_{0.1})O_{5.3}$. Therefore, it can be concluded that annealed Ag10 is a mixture of the BIMEVOX phase and $Bi_{14}V_5AgO_{34}$ at 700°C.

Similar measurements were performed at various temperatures. The results are summarized as pseudo-binary phase diagrams in Fig. 7. Li- and Ag-doped $Bi_2VO_{5.5}$ are metastable at intermediate temperatures. At 400°C, thermal decompositions were kinetically suppressed in Li10 and $Bi_2VO_{5.5}$, and the ordering from $\gamma$- to $\alpha$-phase progressed in Li10. The upper limit of the stable region of the BIMEVOX phase was evaluated by DTA. Partial melting of $Bi_2VO_{5.5}$ commenced at 860°C. Figure 8 show the DTA profile of Li10

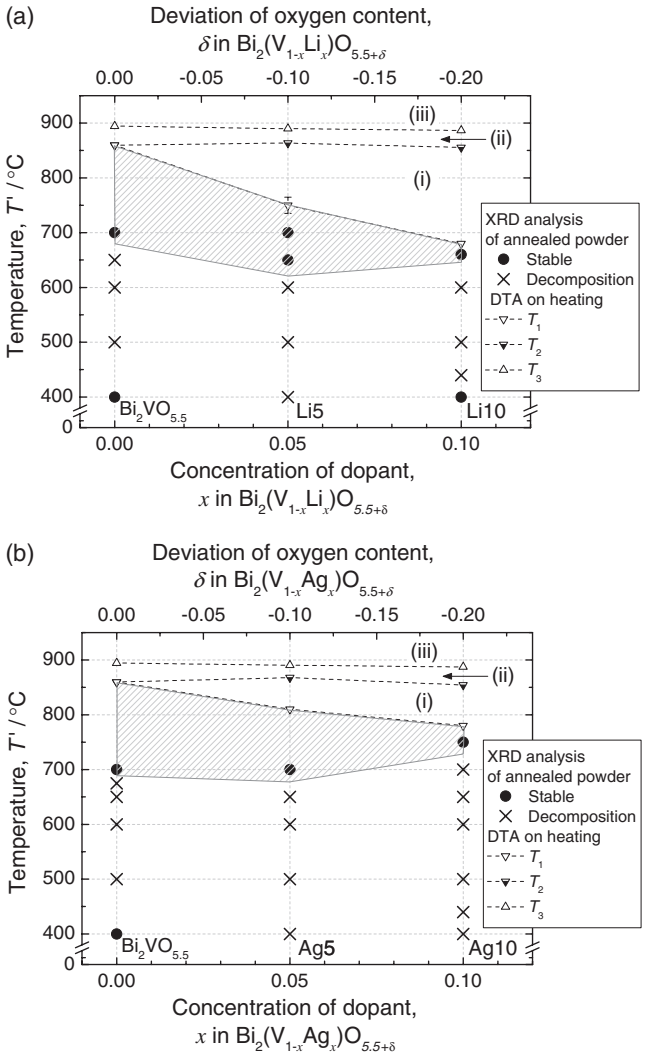


Fig. 7 Pseudo-binary phase diagrams of (a) Li-doped $Bi_2VO_{5.5}$ and (b) Ag-doped $Bi_2VO_{5.5}$. Phase diagrams were generated by the XRD analysis after annealing for 200 h as well as DTA on heating to the temperature at which the liquid phase forms. The shaded areas indicate the thermodynamically stable region of the BIMEVOX phase. An example of a DTA profile is shown in Fig. 8. $T_1$, $T_2$, and $T_3$ represent the onset of a slight endothermic reaction, the onset of a large endothermic reaction, and the end of an endothermic reaction, respectively. Estimated phases in each region are as follows: (i) BIMEVOX phase + small amount of liquid, (ii) solid + liquid, (iii) liquid.

on heating as an example. A slight endothermic reaction started at $T_1 = 680$°C. At the same temperature, an endothermic peak was observed in the DSC profile, as shown in Fig. 1. The DTA profile also shows a large endothermic peak, which appeared at $T_2 = 855$°C, and disappeared at $T_3 = 887$°C. Only the BIMEVOX phase was observed in the HT-XRD profiles at 700 and 750°C, as shown in Fig. 3(b). We confirmed the abnormal grain growth reaching 0.1 mm in grain size by maintaining a Li10 pellet at 800°C for 9 h. Therefore, in the region (i) of Fig. 7 and 8, a small amount of liquid phase was in equilibrium with BIMEVOX phase between $T_1$ and $T_2$. A solid phase quickly melted in the region (ii) above $T_2$, and a single liquid phase was obtained in the region (iii) above $T_3$. The thermodynamically stable region of the BIMEVOX phase, which is indicated by the shaded area in Fig. 7, is reduced by Li- and Ag-doping.

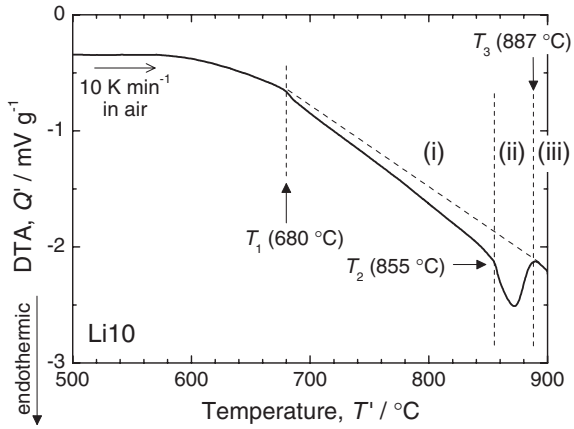


Fig. 8 DTA profile of Li10 on heating at 10 K min$^{-1}$ in air. Estimated phases in each region are as follows: (i) BIMEVOX phase + small amount of liquid, from $T_1$ to $T_2$, (ii) solid + liquid, from $T_2$ to $T_3$, and (iii) liquid, above $T_3$.

## 4. Conclusion

In this study, we investigated the phase transitions and long-term phase stabilities of $Bi_2(V_{1-x}ME_x)O_{5.5+\delta}$ (ME = Li and Ag, $x = 0.05$ and 0.1). Our findings are summarized as follows:

(1) The phase transition behavior is revealed by DSC and HT-XRD analysis. For example, $Bi_2(V_{0.95}Li_{0.05})O_{5.4}$ and $Bi_2(V_{0.95}Ag_{0.05})O_{5.4}$ show transitions from $\alpha$- to $\beta$-phase and $\beta$- to $\gamma$-phase, which explains the changes in electrical conductivity. Both types of 5 mol% doped $Bi_2VO_{5.5}$ showed the similar phase transitions.

(2) The Li- and Ag-doping do not improve the phase stability against thermal decomposition. In $Bi_2(V_{0.9}Ag_{0.1})O_{5.3}$, thermal decomposition is easily occurred even during HT-XRD analysis, which explains the distinct change in electrical conductivity. On the basis of the XRD analysis after long-term annealing for 200 h, $Bi_2(V_{1-x}ME_x)O_{5.5+\delta}$ is confirmed to be metastable at around 500°C.

(3) We generated a pseudo-binary phase diagram as a function of dopant concentration. The stable region of the BIMEVOX phase is reduced by Li- and Ag-doping.

At around 500°C, Li- and Ag-doped $Bi_2VO_{5.5}$ show the highest oxide-ion conductivities among solid oxides. Practical use of these compounds is, however, difficult owing to poor thermal stabilities.

## Acknowledgements

This work was financially supported by a Grant-in-Aid for JSPS fellows.

## REFERENCES

1) F. Abraham, J. C. Boivin, G. Mairesse and G. Nowogrocki: Solid State Ionics **40–41** (1990) 934.
2) J. C. Boivin and G. Mairesse: Chem. Mater. **10** (1998) 2870.
3) N. M. Sammes, G. A. Tompsett, H. Näfe and F. Aldinger: J. Eur. Ceram. Soc. **19** (1999) 1801.
4) G. Mairesse: C. R. Acad. Sci. Paris, Ser. IIc **2** (1999) 651.

5) F. Abraham, M. F. Debreuille-Gresse, G. Mairesse and G. Nowogrocki: Solid State Ionics **28–30** (1988) 529.
6) G. Mairesse, P. Roussel, R. N. Vannier, M. Anne, C. Pirovano and G. Nowogrocki: Solid State Science **5** (2003) 851.
7) G. Mairesse, P. Roussel, R. N. Vannier, M. Anne and G. Nowogrocki: Solid State Science **5** (2003) 861.
8) Y. Taninouchi, T. Uda, T. Ichitsubo, Y. Awakura and E. Matsubara: Collected Abstracts of the 2009 Autumn Meeting of the Japan Inst. Metals (2009) p. 503.
9) J. Van Herle, A. J. Mcevoy and K. R. Thampi: J. Mater. Sci. **29** (1994) 3691.
10) S. Zha, C. Xia and G. Meng: J. Power Sources **115** (2003) 44.
11) T. Ishihara, H. Furutani, M. Honda, T. Yamada, T. Shibayama, T. Akbay, N. Sakai, H. Yokokawa and Y. Takita: Chem. Mater. **11** (1999) 2081.
12) A. Watanabe: J. Solid State Chem. **161** (2001) 410.
13) M. C. Steil, F. Ratajczak, E. Capoen, C. Pirovano, R. N. Vannier and G. Mairesse: Solid State Ionics **176** (2005) 2305.
14) R. D. Shannon: Acta Crystallogr. Sec. A **32** (1976) 751.
15) J. E. Huheey, E. A. Keiter and R. L. Keiter: *Inorganic Chemistry–principles of structure and reactivity*, 4th ed., (Hapere Collins, New York, 1993).